ACS Catalysis

Research Article

pubs.acs.org/acscatalysis

Noninvasive Spatiotemporal Profiling of the Processes of Impregnation and Drying within Mo/Al_2O_3 Catalyst Bodies by a Combination of X-ray Absorption Tomography and Diagonal Offset Raman Spectroscopy

Emma K. Gibson,[†] Mathijs W. Zandbergen,[†] Simon D. M. Jacques,*[,‡] Cai Biao,[‡] Robert J. Cernik,[‡] Matthew G. O'Brien,[†] Marco Di Michiel,[§] Bert M. Weckhuysen,*[,†] and Andrew M. Beale*[,†]

[†]Inorganic Chemistry and Catalysis, Debye Institute for Nanomaterials Science, Utrecht University, Universiteitsweg 99, 3584 CG Utrecht, The Netherlands

[‡]The School of Materials, The University of Manchester, Manchester, M13 9PL, U.K.

[§]The European Synchrotron Facility, 6 Rue Jules Horowitz, 38000, Grenoble, France

Supporting Information

ABSTRACT: A combination of X-ray absorption microcomputed tomography (μ-CT) and diagonal offset raman spectroscopy (DORS) have been used to follow in real time the 2-D and 3-D evolution of Mo species within 3 mm γ-Al_2O_3 extrudates during catalyst impregnation and drying processes. In a first set of experiments, we have followed the real-time incipient wetness impregnation process using an aqueous solution of ammonium heptamolybdate (AHM). We observed that during the equilibration period, singly impregnated samples formed $Al(OH)_6Mo_6O_{18}^{3-}$ (Al–Mo) hot spots distributed over the entire sample volume and that these heterogeneities grow in number and size as a function of time. A second set of measurements focused on the coimpregnation of AHM with H_3PO_4 and the subsequent equilibration and drying stages. It was found that the presence of phosphorus in the impregnating solution prevented the formation of the hot spots via the formation of weakly bound $H_xP_2Mo_5O_{23}^{(6-x)-}$ species that were uniformly distributed over the sample after 70 min of equilibration. During drying, however, these species migrated to the periphery of the sample, resulting in an egg shell distribution of $H_xP_2Mo_5O_{23}^{(6-x)-}$. We show that by performing these studies noninvasively with a sufficiently high time resolution, the behavior and evolution of the Mo species were reproduced more faithfully than by using more conventional and invasive cut-and-measure approaches.

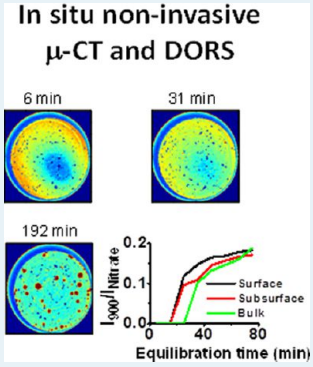

KEYWORDS: *catalyst bodies, spatially resolved, in situ, incipient wetness impregnation*

INTRODUCTION

Heterogeneous catalysts are commonly used in the form of metals or metal oxides dispersed on porous support materials in processes, such as oil refining, emission control, and the manufacturing of bulk and fine chemicals. To ensure against a pressure buildup across industrial reactors, these catalysts are required to be used in the shape of micrometer- to millimeter-sized catalyst bodies. In addition to the oxidation state and coordination environment of the metal/metal oxide species, their speciation and microdistribution are known to greatly influence the overall catalyst efficiency and stability.[1−3] The active phase distribution can be optimized for the process required; for example, uniform or nonuniform microdistributions. Nonuniform distributions include egg shell (the active phase is located at the outer part of the catalyst body), egg white (a gradient of the active phase toward the core of the extrudate), and egg yolk (a gradient of the active phase outward from the core of the extrudate) as shown in Figure S1 of the Supporting Information.[3] Knowing the active phase distribution and its chemical speciation is of vital importance for optimizing catalyst lifetime and activity.

To determine why certain active phase distributions arise, the possible controlling factors, such as impregnation, equilibration, and drying stages, can be investigated; however, current techniques used to study the interactions between the active species and the support in catalyst bodies are subject to limitations. For example, Raman, UV–vis, and IR microspectroscopies require that the samples must be bisected before measurement to investigate the interior of the catalyst body and are therefore invasive.[4] On the other hand, magnetic resonance imaging (MRI),[5] X-ray microscopy, and diffraction imaging[6−10] are noninvasive techniques, but they also have their limitations. MRI, for example, is limited to providing information on only a select number of nuclei and, as such, may be able to yield only indirect information (e.g., ^{1}H NMR of the H_2O coupled

Received: November 18, 2012
Revised: January 11, 2013
Published: January 15, 2013

complex of the catalytically important component) and, furthermore, is primarily applicable for the study of impregnation and drying.[11] In contrast, diffraction-based techniques, such as TADDI/TEDDI (tomographic angle-/energy-dispersive diffraction imaging), are limited to providing information on the crystalline materials present, although the latter technique also yields elemental compositional information for atoms when $Z > 40$.[12] X-ray absorption tomography, although it gives high spatial resolution and is not dependent on the degree of sample crystallinity, provides only elemental contrast images, although it can provide such information with high temporal resolution.[13,14] A method that overcomes the limitations of these techniques providing chemical speciation and doing so noninvasively is diagonal offset Raman spectroscopy (DORS).[15]

Until now, in situ Raman spectroscopy[16−21] has been performed to monitor reactions on the surface of catalyst bodies or to study processes in reactors. Bulk measurements for a variety of applications, however, are now possible as a result of the recently developed spatially offset raman spectroscopy (SORS)[22−25] and time-resolved surface enhanced Raman spectroscopy (TR-SERS).[26] SORS is carried out by collecting a series of Raman spectra while varying the spatial offset, the distance, between the laser and collection optics. Each spectrum contains different contributions of the surface and subsurface layers, which can be separated using multivariate analysis.[22] This technique has been demonstrated on layered turbid media, finding special interest in biological and security screening applications.[27] DORS is a recent modification of SORS, which has been demonstrated for the spatiotemporal in situ study of catalyst bodies. For this application, the laser and collection optics are fixed at a 90° angle to one another, and the sample is moved along the 45° radial line, diagonally between the two. The catalyst body can be rotated and varied in height, thus allowing all parts of the sample to be measured. Previous work by our group has shown the DORS technique can be used to follow dynamically the impregnation of ammonium heptamolybdate on 3 mm γ-Al_2O_3 cylindrical extrudates, and because fluorescence was not an issue for these samples, the DORS technique was chosen for this study.[15]

Here, we have employed the DORS method in combination with X-ray absorption μ-CT for time-resolved in situ investigation of the impregnation and drying stages of molybdenum species on 3 mm cylindrical γ-Al_2O_3 catalyst bodies in a noninvasive manner. The impregnation of molybdenum is the first step in the preparation of (Co)MoS or (Ni)MoS hydrotreating catalysts used for the removal of sulfur, nitrogen, and metals from fuel streams.[28] The impregnation of ammonium heptamolybdate solutions at high concentration, low pH, or long equilibration times are known to lead to the dissolution of the Al_2O_3 surface and formation of $Al(OH)_6Mo_6O_{18}^{3-}$, an Anderson type heteropolyanion (Al−Mo) which in turn forms MoO_3 on calcination.[29,30] Additives (i.e., citrate) can be used to increase the solubility of the metal−ion complex and so limit the precipitation of Mo species, as has been studied previously.[31] Phosphate is also proposed to have beneficial effects on molybdenum-based hydrotreating catalysts; however, the exact nature of its role is still under debate.[32−34] A combination of effects, such as the lower affinity of Mo−P species for the Al_2O_3 and the formation of an $AlPO_4$ layer over which Mo species are less strongly attracted, have been proposed to aid in producing a more uniform Mo distribution.[31,34]

The addition of the H_3PO_4 to the AHM impregnating solution has been previously investigated by our group using Raman microspectroscopy on bisected catalyst bodies.[31,35] Bergwerff et al. found that Al−Mo was formed on the outer surface of the extrudates as a result of a high local Mo concentration and higher acidity, which could be avoided by the addition of sufficient phosphate.[31] Phosphate was also found to aid the preparation of CoMo−Al_2O_3 catalysts when added in excess and in combination with citrate by avoiding the disintegration of the desired $H_2PMo_{11}CoO_4^{5-}$ heteropolyanion and therefore also the formation of Al−Mo.[35] In this work, we report the spatiotemporal investigation of the preparation Mo/γ-Al_2O_3 cylindrical extrudates using DORS to retrieve in situ chemical information from the surface, subsurface, and the bulk; 2-D backscatter Raman spectroscopy (2-D-RS) for 2-D chemical analysis of a bisected extrudate after drying; and μ-CT for in situ 3-D tomographic information on the position of Mo during the equilibration and drying stages. The noninvasive techniques have allowed us to investigate separately the equilibration and drying stages in an attempt to elucidate the chemistry behind the origins of the Mo dispersion.

MATERIALS AND METHODS

Mo(VI) impregnation solutions with 1.3 M Mo concentration were prepared with ammonium heptamolybdate (AHM) (99%, Acros Organics) as the Mo precursor. Ammonium nitrate (0.75 M, 99+%, Antonides) was added to the impregnation solution to provide an internal standard for the DORS measurements. Phosphoric acid (85%, Fisher Scientific) was added to the impregnating solution where appropriate (0.65 M).

Cylindrical γ-Al_2O_3 pellets (Engelhard, 3 mm in diameter and height) were impregnated using the incipient wetness technique. Before impregnation, the pellets had been calcined in air at 450 °C for 8 h and stored at 120 °C afterward. The support had a pore volume of 1.0 mL/g and a surface area of 200 m^2/g.[36] Its point of zero charge (pzc) of 7.8 was determined previously by mass titration.[37] The catalyst bodies were prepared by adding the solution in 10% excess to the pore volume as drops to the pellets. The catalyst bodies as studied by 2-D-RS were prepared by adding the solution in 10% excess to the pore volume as drops to the pellets. The pellets were then shaken manually for 2 min to ensure an even distribution on the pellet surfaces. Afterward, the 10% excess solution was removed, and wet tissue was added to the storage vessel to avoid drying during equilibration. The impregnation of the pellets used during the DORS measurements was performed in a glass container, as described elsewhere.[15] A total of 220 μL of impregnation solution was added to the pellet as evenly as possible with a syringe. After impregnation, the holder was covered to keep the environment of the extrudate humid. The DORS measurements were started 1−5 min after the impregnation.

The DORS setup has been described in detail elsewhere.[15] A tunable 300 mW 532 nm laser with a spot size of ∼100 μm was used during the DORS measurements. The laser power was set to be 35 mW on the sample. Collection optics were used to obtain a collection spot size of ∼200 μm. The laser, laser and collection optics, and the collection software were provided by Cobalt Light Systems. Motion link series 2000 stage linear travel stages were used for *XYZ*, and a MICOS DT65N for the rotation stage. A Kaiser Grams/Holograms data acquisition system was used to record the Raman spectra. The collection time was set at 10 s, with three accumulations per measure-

dx.doi.org/10.1021/cs300746a | *ACS Catal.* 2013, 3, 339−347

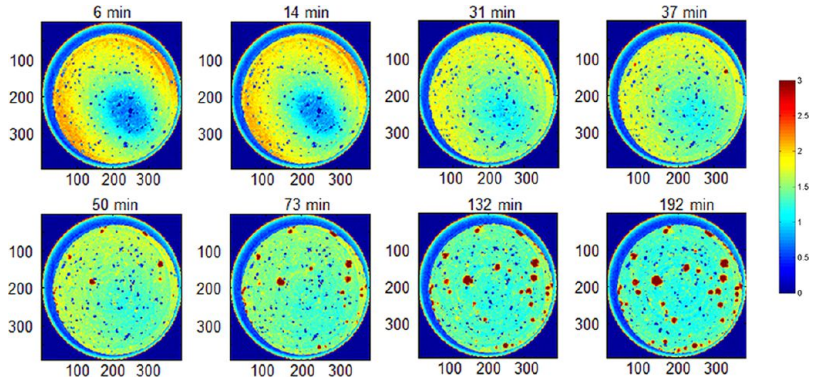

Figure 1. 2-D X-ray absorption μ-CT cross section thermal plots (red = high concentration, blue = low) of a slice of a γ-Al_2O_3 extrudate after incipient wetness impregnation of a 1.3 M Mo ammonium heptamolybdate solution at pH 5 as a function of time. The units for the color bar on the right-hand side of the figure are cm^{-1}.

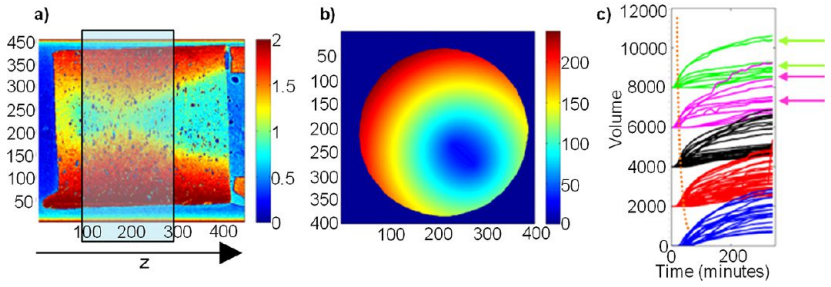

Figure 2. (a) Longitudinal μ-CT section through the extrudate near time zero showing an uneven impregnation in the Z direction (color bar units are cm^{-1}), (b) map of the convergence distances (distance from any point to the convergence center, as described in the Supporting Information) in units of number of pixels from two foci points, and (c) the 500 hot spots grouped according to distance from the convergence center.

ment. Three $x-y$ positions of the sample were used to yield information on the extrudate surface, subsurface, and bulk. The point of illumination and the point of collection overlap for the first position (surface). The distance between these two points increases by 0.75 mm for the second position (subsurface) and 1.5 mm for the third position (bulk). The spatial resolution is close to the spot size for a surface DORS measurement. Because of multiple scattering of photons through the sample, it increases to the millimeter range when the bulk is measured.[38]

2-D backscatter Raman maps of the bisected extrudates were also obtained by a Raman scanning method developed in-house. These were performed on the surface of bisected pellets at 100 μm intervals. For laser generation in backscattered mode, a Kaiser RamanRxn1 equipped with a 532 nm diode laser and with a Kaiser Mk II filtered probe with a lens system with a focal distance of 8 cm was used. The power of the beam from the probe was 15 mW. The collection time was 1 s, averaged over three acquisitions for these measurements. DORS and backscattered data were preprocessed using FileConv, then analyzed using a combination of the EasyDD and Matlab.[14,39,40]

μ-Absorption-CT experiments were performed at station ID15A of the ESRF (Grenoble, France) using a monochromatic X-ray beam (energy = 69.77 keV). Measurements were recorded using a high-resolution imaging detector made of a LuAg/Ce scintillator (125 mm thick) to convert the X-ray absorption into a visible light image (wavelength ~ 550 nm), focusing optics ($2x-5x$), and a Dalsa Pantera 1M60 CCD camera (1024 × 1024 pixels, pixel size 14 μm) to record the image. Reconstruction results in a 3-D tomogram with a resolution of ~5 μm per pixel (H × V). The cell used has been described elsewhere.[8]

RESULTS AND DISCUSSION

1. Processes of Impregnation with AHM. The incipient wetness impregnation with 1.3 M Mo has been investigated in situ in real time using both μ-CT and DORS. The time-resolved μ-CT data are shown in Figure 1. It was observed that Mo complexes slowly migrate toward the center of the extrudate during equilibration, forming an egg white type of distribution after 30 min, with a gradient of high to low Mo concentration from the outer edge toward the center of the extrudate. From 31 min onward, high concentrations, hereby termed "hot spots" of Mo species were observed. Note, however, that the center of the sample did not contain hot spots. With longer equilibration times, the hot spots grew in number and size so that after 37 min, they are shown to be well-distributed throughout the whole body of the extrudate (Figure 2). From these images, the range in volume of the hot spots can be clearly observed.

To determine insight into the nucleation and growth of the hot spots, numerical modeling of the growth of some ~500 of these during equilibration was performed from a volume defined by the rectangle shown in Figure 2a. Hot spots that were found to coalesce during growth, particularly at the periphery of the extrudate, were excluded from the analysis so as to yield information only on the nucleation and growth process. A convergence center was defined as described in detail in the Supporting Information, allowing correlation of particle position with respect to the region of low initial Mo

dx.doi.org/10.1021/cs300746a | ACS Catal. 2013, 3, 339−347

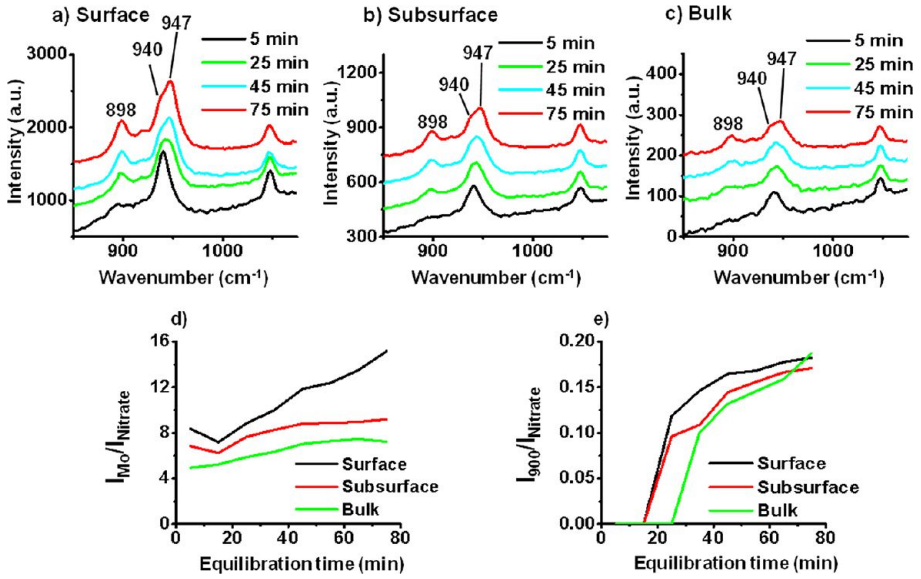

Figure 3. In situ DORS measurement of the (a) surface, (b) subsurface, and (c) bulk of a γ-Al_2O_3 extrudate after incipient wetness impregnation of a 1.3 M Mo ammonium heptamolybdate solution at pH 5 as a function of equilibration time. The ratio (d) of intensities of Mo species (900−1000 cm^{-1}) against NO^{3-} (1050 cm^{-1}) and (e) the ratio of intensity of the 900 cm^{-1} band (Al−Mo) against the combined intensities of the Al−Mo and heptamolybdate bands (936, 940, and 947 cm^{-1}) vs equilibration time.

concentration to be established. A map of the distances to this convergence center is shown in Figure 2b.

From Figure 2c, it is clear that the final hot spot volumes are independent of location and that these varied in size across all regions of the extrudate. In addition, an induction time is observed that is greater for hot spots growing closer to the convergence center, where the concentration of Mo was initially low. Furthermore, no evidence of Oswald ripening was observed, since all 500 particles analyzed grew continually in size and were not observed to dissolve.[41] A more detailed analysis and discussion of the particle growth process is given in the Supporting Information.

With X-ray absorption μ-CT, the migration of the molybdenum species during the dynamic equilibration process and the formation of hotspots can be followed, but to determine the chemical nature of the species that gives rise to the Mo egg white distribution and the hot spots, in situ DORS measurements were performed in a parallel experiment. For these measurements, NH_4NO_3 was also added to the solution to provide an internal standard (the Raman band of NO^{3-} at 1050 cm^{-1}), since previously, it was shown that the nitrate anion is homogeneously distributed after 10 min equilibration time. The parallel DORS data for the impregnation process are shown in Figure 3a−c for the surface, subsurface, and bulk, respectively. At the beginning of the equilibration process, Mo was observed to be present as $Mo_7O_{24}^{6-}$, as evidenced by a Raman band at 940 cm^{-1}. This band appeared at a lower wavenumber than that found in the impregnating solution because of the increase in the pH (to ~5.5) of the solution in the pores caused by contact/protonation of the surface hydroxyl groups forming $Al{-}OH^{2+}$ on the γ-Al_2O_3 support. After 30 min, $Mo_7O_{24}^{6-}$ reacts with the support under acidic conditions[29−31,35,42,43] to form $Al(OH)_6Mo_6O_{18}^{3-}$ (eq 1), an Anderson type heteropolyanion, with Raman bands at 570, 898, and 947 cm^{-1}, referred to as Al−Mo from now on.[29,30,42,43]

$$12Mo_7O_{24}^{6-} + 7Al_2O_3 + 27H_2O + 30H^+ \rightarrow 14Al(OH)_6Mo_6O_{18}^{3-} \quad (1)$$

With increasing equilibration time, the intensity of the Raman band for Al−Mo increases relative to that of nitrate and $Mo_7O_{24}^{6-}$ (Figure 3d and e, respectively) because more of this species is formed. It is likely that this Al−Mo phase is the "hot spot" species seen in the μ-CT data. However, we observe a discrepancy of 15 min between the observations made using the two techniques, which is thought to originate from heating of the extrudate during laser exposure (5 min every 10 min) when performing DORS, which, although did not lead to drying of the surface, does appear to accelerate formation of Al−Mo. For example, hot spots of Al−Mo are observed after 31 min by μ-CT, but after only 15 min using DORS (Figure 3e). A higher $I_{Mo}/I_{nitrate}$ ratio is observed at the surface than in the bulk, indicating a higher concentration of Mo species (the combined concentration of both Al−Mo and $Mo_7O_{24}^{6-}$) is present near the exterior of the extrudate than in the bulk, as confirmed by μ-CT. The ratio between the intensity of the band at 900 cm^{-1} and that of the combined bands at 936, 940, and 947 cm^{-1} also increases with equilibration time. However, this increase is delayed in the bulk, that is, the increase does not start until 25−35 min of equilibration, as observed by DORS in the bulk. Formation of Al−Mo therefore starts near or at the surface of the extrudate because of the higher concentration of $Mo_7O_{24}^{6-}$ initially observed in that area (Figure 3).

A strong electrostatic interaction between the negatively charged $Mo_7O_{24}^{6-}$ and the positively charged $Al{-}OH^{2+}$ support is the likely cause of inhibition of impregnation toward the center of the extrudate.[31,35] A high concentration of $Mo_7O_{24}^{6-}$ near the surface of the extrudate would likely push the equilibrium in reaction 1 toward the right-hand side, resulting in the formation of Al−Mo hot spots and the observed egg shell microdistribution of Al−Mo (Figure 3d). A schematic representation of the impregnation process and

dx.doi.org/10.1021/cs300746a | ACS Catal. 2013, 3, 339−347

reaction of the AHM with the hydrated alumina surface to form Al−Mo species is shown in Figure 4.

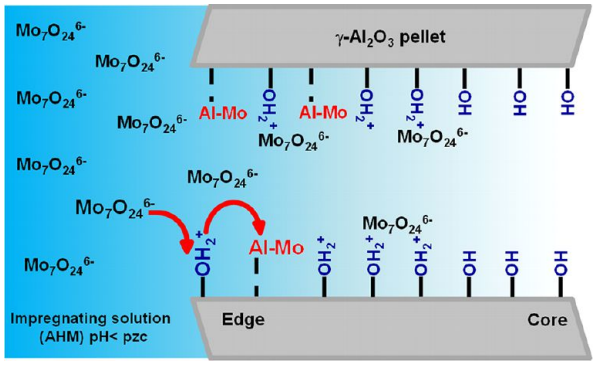

Figure 4. A schematic representation of the diffusion of the AHM solution into the pores of the γ-Al_2O_3 extrudate, showing the reaction of the hydrated alumina surface with the AHM to form Al−Mo as the AHM concentration gradient passes through the pore. The Al−Mo species form initially in regions of high AHM concentration.

The formation of hotspots of Al−Mo was not reported previously by Bergwerff et al. when γ-Al_2O_3 extrudates were impregnated with similar solutions.[31] The support used in that study had a higher point of zero charge (8.8−9.0), and therefore, the buffering effect is stronger, resulting in a higher solution pH in the pores and different Mo speciation; $Mo_7O_{24}^{6-}$ is present mainly at solution pH of 5−6, whereas MoO_4^{2-} is predominant at pH > 6.[44] Because of the higher buffering influence of the support, $Mo_7O_{24}^{6-}$ was converted to mostly MoO_4^{2-} inside the pores. Without $Mo_7O_{24}^{6-}$, reaction 1 does not occur, and hot spots of Al−Mo do not form; however, Bergwerff et al. did observe Al−Mo on the outside surface of the extrudates, which can be explained by the higher concentration of $Mo_7O_{24}^{6-}$ and favorable pH at this location.

Extrudates bisected after 2.5, 30, and 125 min of equilibration and subsequent drying overnight were analyzed by 2-D Raman mapping (Figure 5).[15] The 2-D Raman data confirm that Al−Mo is found predominantly in the form of hot spots at or near the exterior of the extrudate in what can be described as an egg white distribution. The center also contains Al−Mo but at a lower concentration. The radius of the hot spot free center decreases with equilibration time, from 1 mm after 2.5 min to 0.5 mm after 125 min. Interestingly, these results are not in agreement with the DORS and μ-CT measurements performed in situ, where hot spot formation was observed only after ∼30 min equilibration time. This discrepancy between the results of the 2-D-Raman and the in situ studies (μ-CT and DORS) can almost certainly be attributed to the effect of drying. The process of bisecting and measurement of the extrudate appears then to alter the microdistribution of Al−Mo, leading to a higher number of Al−Mo hot spots. It should be noted that the contradiction between 2-D Raman and μ-CT results cannot be explained by a difference in resolution because the resolution is, in fact, much higher for μ-CT (2 μm) compared with 2-D Raman (100 μm).

2. Impregnation with AHM and H_3PO_4. Figure 6 contains the 2-D μ-CT x−z slices detailing the change in distribution of Mo species with equilibration time. Thirty seconds after impregnation an egg shell distribution was observed, showing that the Mo species have not yet reached the inner core of the extrudate. The distribution became egg white after 30 min, and finally, a uniform distribution was achieved after 70 min. The DORS measurements show that at the surface, only $H_xP_2Mo_5O_{23}^{(6-x)-}$ is present, with Raman bands located at 370, 395, 885, and 936 cm^{-1}.[31,35] The Raman band due to $H_xP_2Mo_5O_{23}^{(6-x)-}$ shifts slightly toward a lower wavenumber from 939 to 936 cm^{-1} (observed most clearly

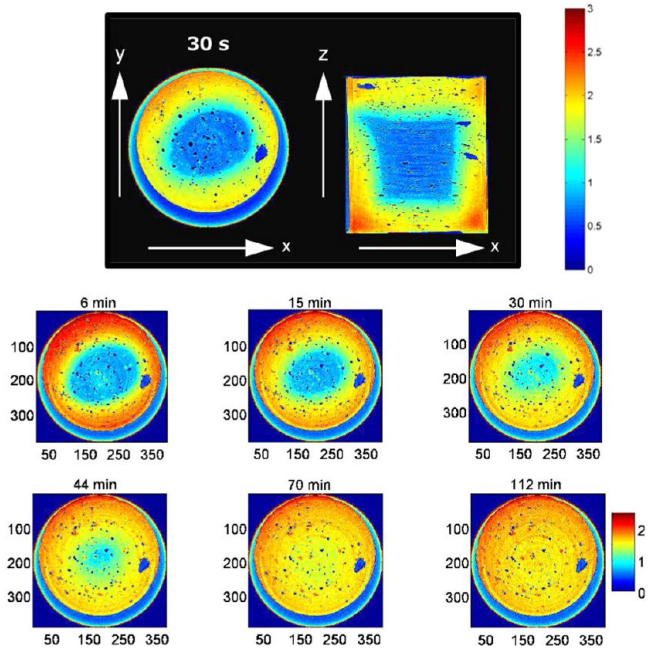

Figure 6. 2-D X-ray absorption μ-CT images of a slice of a γ- Al_2O_3 extrudate after incipient wetness impregnation of a 1.3 M Mo ammonium heptamolybdate solution containing 0.65 M H_3PO_4 at pH 2 after 30 s equilibration . The 2-D x−y slice is shown as a function of equilibration time (with color bar in units of cm^{-1}).

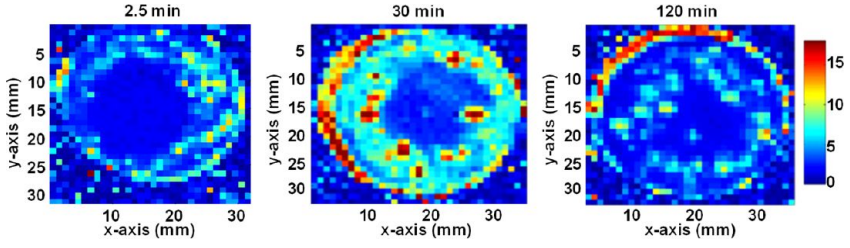

Figure 5. 2-D Raman maps of the I_{Mo}/I_{NO_3} of the γ-Al_2O_3 extrudates after incipient wetness impregnation with a 1.3 M Mo ammonium heptamolybdate solution at pH 5 removed from equilibration environment after 2.5, 30, and 120 min. Units for the color bar on the right are Raman scattering intensity (a.u.).

dx.doi.org/10.1021/cs300746a | ACS Catal. 2013, 3, 339−347

for the surface spectra, Figure 7a). This shift can be explained by the increase in pH of the solution in the pores due to the

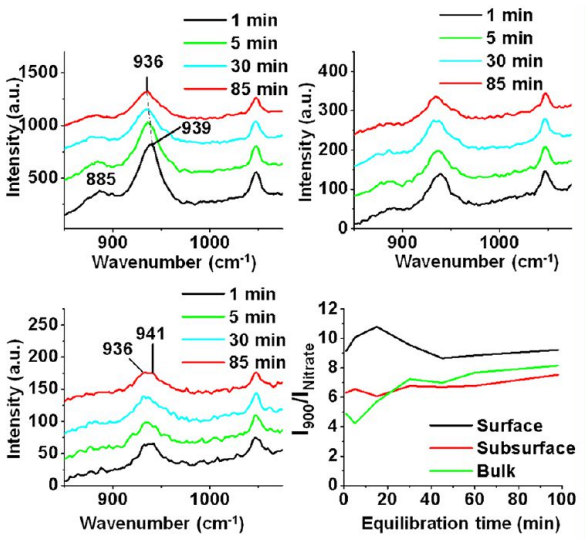

Figure 7. Raman spectra in DORS mode of a γ-Al_2O_3 extrudate after incipient wetness impregnation of a 1.3 M Mo ammonium heptamolybdate solution containing 0.65 M H_3PO_4 at pH 2 as a function of time. $H_xP_2Mo_5O_{23}^{(6-x)-}$ is denoted by the bands at 936 and 885 cm^{-1}, and $Mo_7O_{24}^{6-}$, by the band at 941 cm^{-1}.

reaction of free phosphate with the alumina to form $AlPO_4$ layers, (eq 2); this increase in pH leads to a deprotonation of the $H_xP_2Mo_5O_{23}^{(6-x)-}$ species (Table 1).[32] We also observed a

Table 1. Characteristic Vibrations of the Mo Species Measured in Solution[31]

pH	species	ν (MoO_{2t})	δ (MoO_{2t})
2	$H_xP_2Mo_5O_{23}^{6-x-}$	942, 893	395, 370
4	$H_xP_2Mo_5O_{23}^{6-x-}$	936, 884	395, 370
6	$P_2Mo_5O_{23}^{6-}$	956, 926, 874	395, 370
5.5	$Mo_7O_{24}^{6-}$	941, 896	358
higher pH	MoO_4^{2-}	896, 836	320

shoulder at 940 cm^{-1}, which can be attributed to Mo present as $Mo_7O_{24}^{6-}$ and was observed most clearly in the bulk spectrum recorded after 85 min. The formation of this species can be explained as a result of a low local concentration of free phosphate due to reaction 2, resulting in the disintegration of Mo−P species. As reaction 2 occurs, the concentration of free phosphate toward the center of the extrudate would decrease, and the pH in the pores would increase so as to destabilize the $H_xP_2Mo_5O_{23}^{(6-x)-}$ and shift the equilibrium (eq 3) to the right.[31] This would produce more free phosphate, which is able to further react with the alumina support. Physisorption of both $H_xP_2Mo_5O_{23}^{(6-x)-}$ and $Mo_7O_{24}^{6-}$ has previously been demonstrated to be possible over the $AlPO_4$ layer.[45]

$$Al_sOH + HPO_4^{2-} + H^+ \leftrightarrow AlHPO^{4-} + H_2O \quad (2)$$

$$7P_2Mo_5O_{23}^{6-} + 15H_2O \leftrightarrow 5Mo_7O_{24}^{6-} + 14HPO_4^{2-} + 16H^+ \quad (3)$$

The ratio of the intensity of the Mo band ($\sim$ 936 cm^{-1}) against that of the nitrate showed a concentration gradient existed across the sample until almost 60 min equilibration time; however, after 60 min, the concentration of Mo species was observed to be almost equal across the entire sample, as evidenced in both the DORS and μ-CT data. A uniform Mo−P species distribution and the presence of $Mo_7O_{24}^{6-}$ at the core were also observed for samples impregnated with a 2:1 ratio of Mo/P and equilibrated for 360 min by Bergwerff et al.[31]

3. Effect of Drying. The drying of an extrudate impregnated with a 1.3 M Mo ammonium heptamolybdate solution containing 0.65 M H_3PO_4 and left to equilibrate for 80 min was investigated using μ-CT, as illustrated in Figure 8. The

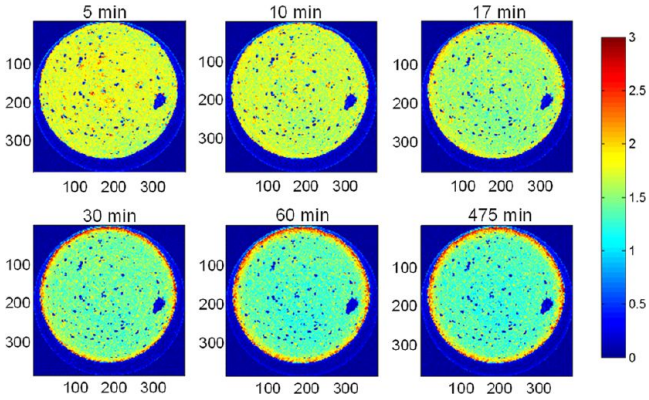

Figure 8. X-ray absorption μ-CT of a slice of a γ-Al_2O_3 extrudate after incipient wetness impregnation of a 1.3 M Mo ammonium heptamolybdate solution containing 0.65 M H_3PO_4 at pH 2 as a function of time of drying in air at RT (with color bar in units of cm^{-1}).

distribution of Mo−P species was initially homogeneous, as observed during the impregnation process. After 17 min of drying, however, the concentration of Mo near the edge of the extrudate started to increase, resulting eventually in an egg shell distribution after 30 min. This could be due to the evaporation of water from the pores, pulling out with it the weakly adsorbed Mo−P species.[45] Indeed, numercial models have been determined to describe the effects of drying on weakly adsorbed and strongly adsorbed species, with the former found to be more susceptible to change in distribution during drying compared with systems that are strongly adsorbed, where the distribution is mostly determined during the impregnation step.[46] Other systems in the literature also realized the formation of an egg shell distribution on drying, such as in the case of Ni/γ-Al_2O_3 and $Cu(NO_3)_2$ on α-Al_2O_3.[46−48] Backscatter Raman measurements at the surface of a sample treated in a similar fashion confirm that the molybdenum species at the egg shell are Mo−P, having bands at 364, 390, 880, and 934 cm^{-1}.

Samples removed from equilibration at 30 and 125 min and dried overnight were bisected to perform 2-D Raman measurements. These results are summarized in Figure 9. After 30 min, the sample exhibited an egg white distribution of $H_xP_2Mo_5O_{23}^{(6-x)-}$, with bands located at 370, 396, 884, and 936 cm^{-1}; however, the core contains bands at 936 and 950 cm^{-1}, signifying a mixture of $H_xP_2Mo_5O_{23}^{(6-x)-}$ and Al−Mo species, with the latter being of higher intensity. After 125 min equilibration, the resulting extrudate shows an egg shell distribution of $H_xP_2Mo_5O_{23}^{(6-x)-}$ after drying. The results

dx.doi.org/10.1021/cs300746a | ACS Catal. 2013, 3, 339−347

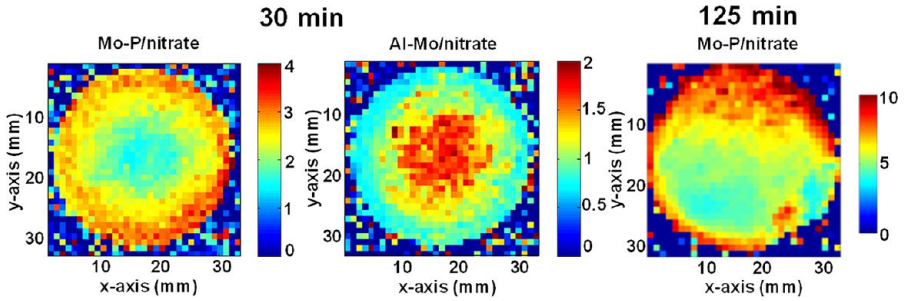

Figure 9. 2-D Raman measurements of extrudates after incipient wetness impregnation of a 1.3 M Mo ammonium heptamolybdate solution containing 0.65 M H_3PO_4 at pH 2 removed from the equilibration environment after 30 and 125 min and left to dry at RT overnight, before bisection.

obtained after 30 min equilibration, drying, and bisection are in agreement with the μ-CT and DORS. The in situ experiments showed the formation of a small amount of $Mo_7O_{24}^{6-}$ at the core of the extrudate after long equilibration times (85 min), we can postulate this $Mo_7O_{24}^{6-}$ would be less easily redistributed on drying and, if in high enough concentration, lead to the formation of Al−Mo. Because the in situ μ-CT drying experiment was performed after longer equilibration times, the slow phosphate migration, as measured previously in γ-Al_2O_3 pellets by ^{31}P NMR,[49] could have caught up with the molybdenum species and once again formed Mo−P species that are more easily redistributed on drying.

A schematic representation of the transport of AHM and phosphoric acid into the pores of the Al_2O_3 extrudate is shown in Figure 10a, showing the reaction of the phosphate with the alumina surface to form $AlPO_4$ layers, adsorption of the weakly bound Mo−P species, and the disintegration of these species to form $Mo_7O_{24}^{6-}$ in areas of low local phosphate concentration. The reaction of the slowly migrating phosphate with $Mo_7O_{24}^{6-}$ to form Mo−P species is also shown. Equilibration of 125 min, drying, and bisection gave an egg white distribution of $H_xP_2Mo_5O_{23}^{(6-x)-}$, confirming that the Mo species observed by μ-CT to migrate to the periphery during drying are $H_xP_2Mo_5O_{23}^{(6-x)-}$, as depicted in Figure 10b. This result would appear to contradict Bergwerff et al., who observed the formation of large quantities of Al−Mo on the outer edge of extrudates impregnated with similar solutions.[31] However, this can be rationalized by comparing the difference in pH inside the pores as observed from the main ν(MoO2t) band of the $H_xP_2Mo_5O_{23}^{(6-x)-}$ species in each system. In this work, the $\nu(MoO_{2t})$ band is observed at 936 cm^{-1}, indicating a pH inside the pores of ∼4. Bergwerff et al. observed the $\nu(MoO_{2t})$ band at 929 cm^{-1} due to a higher extent of deprotonation of the $H_xP_2Mo_5O_{23}^{(6-x)-}$ species, indicating a pH of ∼5. This higher pH and the slower distribution of Mo species inside the extrudate (after 90 min, very little Mo is observed at the core) would lead to a greater concentration of $Mo_7O_{24}^{6-}$ at the external surface and, therefore, the formation of Al−Mo. In this case, the lower buffering effect of the support appears to have an advantageous effect on the stability of Mo−P species and, therefore, the avoidance of Al−Mo.

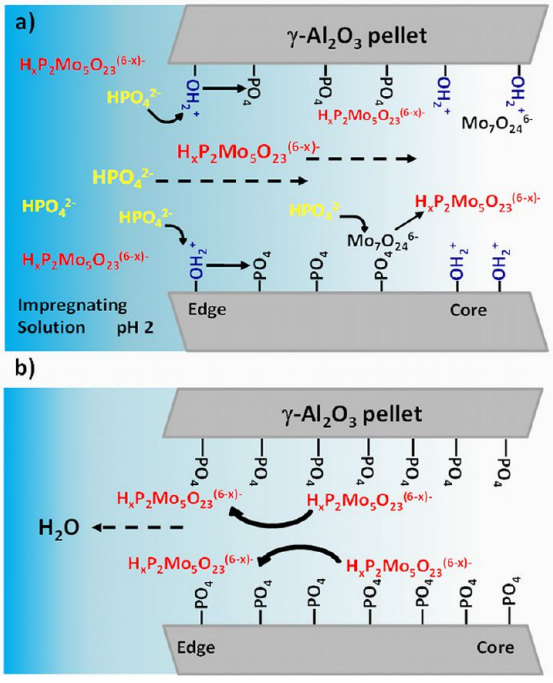

Figure 10. (a) A schematic representation of the transport of AHM and phosphoric acid into the pores of the Al_2O_3 extrudate, showing the formation of $AlPO_4$ layers and adsorption of weakly bound Mo−P species and disintegration to form $Mo_7O_{24}^{6-}$ in areas of low local phosphate concentration. The diffusion of the weakly bound Mo−P species out of the pores on drying is shown in part b, resulting in a final egg shell distribution.

CONCLUSIONS

With the advent of μ-CT and DORS methods for noninvasive investigation of catalyst bodies, which afford spatiotemporal chemical information to be obtained during in situ studies, the importance of revisiting the chemistry of millimeter-sized cylindrical Mo/γ-Al_2O_3 extrudates becomes apparent. The obtained 2-D Raman data highlight the pitfalls of relying on invasive techniques in which snapshots of the combined impregnation and drying processes are taken, leading to an alteration of the chemistry associated with the impregnation process and to possible misinterpretation of the speciation involved in catalyst preparation. By studying separately the equilibration and drying stages, we have shown that the nature and final spatial distribution of the Mo species is determined by both the impregnation and drying stages for AHM-impregnated γ-Al_2O_3 extrudates, whereas for the AHM/H_3PO_4 coimpregnated system the drying stage is the critical step.

The most important findings can be summarized as follows:

- The migration of Mo through the extrudate on impregnation with ammonium heptamolybdate solutions is slow, resulting in an egg white distribution after 30

dx.doi.org/10.1021/cs300746a | ACS Catal. 2013, 3, 339−347

min; however, equilibration times longer than this lead to the formation of Al−Mo hot spots.
- Nucleation of these hot spots is subject to an induction time, being greater for those hot spots forming closer to the area with initially low Mo concentration. This would indicate that a critical concentration of molybdenum is needed before nucleation occurs and, therefore, is a function of the diffusion of the impregnating solution. This is implicit in the stoichiometry of eq 1, where a 6:1 ratio of Mo−Al is needed to form the Al−Mo heteropolyanion.
- Al−Mo hot spot formation is radically accelerated by drying, to such an extent that their formation is observed after equilibration times as short as 2.5 min.
- Co-impregnation of AHM/H_3PO_4 solutions prohibits Al−Mo formation with weakly bound $H_xP_2Mo_5O_{23}^{(6-x)-}$ species observed instead, which is uniformly distributed after a 70 min equilibration period.
- Drying is responsible for the redistribution of these weakly bound species and the final egg white distribution.

■ ASSOCIATED CONTENT

Supporting Information

A detailed description of the μ-absorption-CT and numerical modeling of particle growth. This material is available free of charge via the Internet at http://pubs.acs.org.

■ AUTHOR INFORMATION

Corresponding Author

*E-mail: a.m.beale@uu.nl, b.m.weckhuysen@uu.nl, simon.jacques@gmail.com.

Notes

The authors declare no competing financial interest.

■ ACKNOWLEDGMENTS

The authors thank the Aspect-ACTS programme for financial support.

■ REFERENCES

(1) Marceau, E.; Carrier, X.; Che, M.; Clause, O.; Marcilly, C. In *Handbook of Heterogeneous Catalysis*; Ertl, G., Knoziger, H., Schuth, F., Weitkamp, J., Eds.; Wiley-VCH: Weinheim, 2008; pp 467−484.
(2) Geus, J. W. In *Catalyst Preparation, Science and Engineering*; Regalbuto, J., Ed.; CRC: Boca Raton, 2007; pp 341−370.
(3) Neimark, A. V.; Kheifets, L. I.; Fenelonov, V. B. *Ind. Eng. Chem. Prod. Res. Dev.* **1981**, *20*, 439−450.
(4) van de Water, L. G. A.; Bergwerff, J. A.; Nijhuis, T. A.; de Jong, K. P.; Weckhuysen, B. M. *J. Am. Chem. Soc.* **2005**, *127*, 5024−5025.
(5) Bergwerff, J. A.; Lysova, A. A.; Alonso, L. E.; Koptyug, I. V.; Weckhuysen, B. M. *Angew. Chem., Int. Ed.* **2007**, *46*, 7224−7227.
(6) Grunwaldt, J.-D.; Schroer, C. G. *Chem. Soc. Rev.* **2010**, *39*, 4741−4753.
(7) Ruffino, L.; Mann, R.; Oldman, R.; Stitt, E. H.; Boller, E.; Cloetens, P.; Di Michiel, M.; Merino, J. *Can. J. Chem. Eng.* **2005**, *83*, 132−139.
(8) Jacques, S. D. M.; Di Michiel, M.; Beale, A. M.; Sochi, T.; O'Brien, M. G.; Espinosa-Alonso, L.; Weckhuysen, B. M.; Barnes, P. *Angew. Chem., Int. Ed.* **2011**, *50*, 10148−10152.
(9) Espinosa-Alonso, L.; O'Brien, M. G.; Jacques, S. D. M.; Beale, A. M.; de Jong, K. P.; Barnes, P.; Weckhuysen, B. M. *J. Am. Chem. Soc.* **2009**, *131*, 16932−16938.
(10) Espinosa-Alonso, L.; Beale, A. M.; Weckhuysen, B. M. *Acc. Chem. Res.* **2010**, *43*, 1279−1288.
(11) Koptyug, I. V. *Prog. Nucl. Magn. Reson. Spectrosc.* **2012**, *65*, 1−65.
(12) Betson, M.; Barker, J.; Barnes, P.; Atkinson, T.; Jupe, A. *Transp. Porous Media* **2004**, *57*, 203−214.
(13) Beale, A. M.; Jacques, S. D. M.; Weckhuysen, B. M. *Chem. Soc. Rev.* **2010**, *39*, 4656−4672.
(14) O'Brien, M. G.; Jacques, S. D. M.; Di Michiel, M.; Barnes, P.; Weckhuysen, B. M.; Beale, A. M. *Chem. Sci.* **2012**, *3*, 509−523.
(15) Zandbergen, M. W.; Jacques, S. D. M.; Weckhuysen, B. M.; Beale, A. M. *Angew. Chem., Int. Ed.* **2012**, *51*, 957−960.
(16) Peter, C. *Catal. Today* **1997**, *33*, 353−360.
(17) Wachs, I. E. *Top. Catal.* **1999**, *8*, 57−63.
(18) Trouillet, L.; Toupance, T.; Villain, F.; Louis, C. *Phys. Chem. Chem. Phys.* **2000**, *2*, 2005−2014.
(19) Stair, P. C. *Curr. Opin. Solid State Mater. Sci.* **2001**, *5*, 365−369.
(20) Brückner, A. *Catal. Rev. Sci. Eng.* **2003**, *45*, 97−150.
(21) Banares, M. *Catal. Today* **2005**, *100*, 71−77.
(22) Matousek, P.; Clark, I. P.; Draper, E. R. C.; Morris, M. D.; Goodship, A. E.; Everall, N.; Towrie, M.; Finney, W. F.; Parker, A. W. *Appl. Spectrosc.* **2005**, *59*, 393−400.
(23) Matousek, P.; Morris, M. D.; Everall, N.; Clark, I. P.; Towrie, M.; Draper, E.; Goodship, A.; Parker, A. W. *Appl. Spectrosc.* **2005**, *59*, 1485−1492.
(24) Matousek, P. *Appl. Spectrosc.* **2006**, *60*, 1341−1347.
(25) Schulmerich, M. V.; Dooley, K. A.; Vanasse, T. M.; Goldstein, S. A.; Morris, M. D. *Appl. Spectrosc.* **2007**, *61*, 671−678.
(26) Harvey, C. E.; Petterson, E. I.; Weckhuysen, B. M.; Gooijer, C.; Mank, J. G. *Appl. Spectrosc.* **2012**, *66*, 1179−1185.
(27) Matousek, P. *Chem. Soc. Rev.* **2007**, *36*, 1292−1304.
(28) Lloyd, L. In *Handbook of Industrial Catalysts*; Springer US:: Boston, MA, 2011; pp 211−260.
(29) Le Bihan, L.; Blanchard, P.; Fournier, M.; Grimblot, J.; Payen, E. *J. Chem. Soc. Faraday Trans.* **1998**, *94*, 937−940.
(30) Carrier, X.; Lambert, J.-F.; Kuba, S.; Knözinger, H.; Che, M. *J. Mol. Struct.* **2003**, *656*, 231−238.
(31) Bergwerff, J. A.; Visser, T.; Leliveld, B. R. G.; Rossenaar, B. D.; de Jong, K. P.; Weckhuysen, B. M. *J. Am. Chem. Soc.* **2004**, *126*, 14548−56.
(32) Kraus, H.; Prins, R. *J. Catal.* **1996**, *164*, 251−259.
(33) Sun, M.; Nicosia, D.; Prins, R. *Catal. Today* **2003**, *86*, 173−189.
(34) Iwamoto, R.; Grimblot. *J. Adv. Catal.* **1999**, *44*, 417−503.
(35) Bergwerff, J. A.; van de Water, L. G. A.; Visser, T.; de Peinder, P.; Leliveld, B. R. G.; de Jong, K. P.; Weckhuysen, B. M. *Chem.—Eur. J.* **2005**, *11*, 4591−601.
(36) Espinosa-Alonso, L.; de Jong, K. P.; Weckhuysen, B. M. *J. Phys. Chem. C* **2008**, *112*, 7201−7209.
(37) Noh, J. *J. Colloid Interface Sci.* **1989**, *130*, 157−164.
(38) Everall, N.; Matousek, P.; MacLeod, N.; Ronayne, K. L.; Clark, I. P. *Appl. Spectrosc.* **2010**, *64*, 52−60.
(39) Sochi, T.; Jaques, S. D. M.; Barnes, P.; Easy D. D. software unpublished 2009.
(40) The MathWorks Inc. Commercial software package *MATLAB R2008b*; Natick: MA, 2008.
(41) Datye, A. K.; Xu, Q.; Kharas, K. C.; McCarty, J. M. *Catal. Today* **2006**, *111*, 59−67.
(42) Botto, I.; Garcia, A.; Thomas, H. *J. Phys. Chem. Solids* **1992**, *53*, 1075−1080.
(43) Carrier, X.; Lambert, J. F.; Che, M. *J. Am. Chem. Soc.* **1997**, *119*, 10137−10146.
(44) Bergwerff, J. A.; Visser, T.; Weckhuysen, B. M. *Catal. Today* **2008**, *130*, 117−125.
(45) Van Veen, J.; Hendriks, P.; Andrea, R.; Romers, E.; Wilson, A. *J. Phys. Chem.* **1990**, *94*, 5282−5285.
(46) Lekhal, A.; Glasser, B. J.; Khinast, J. G. *Chem. Eng. Sci.* **2001**, *56*, 4473−4487.
(47) Li, W. D.; Li, Y. W.; Qin, Z. E.; Chen, S. Y. *Chem. Eng. J.* **1994**, *49*, 4889−4895.
(48) Uemura, Y.; Hatate, Y.; Ikari, A. *J. Chem. Eng. Jpn.* **1987**, *20*, 117−123.

(49) Lysova, A. A.; Koptyug, I. V.; Sagdeev, R. Z.; Valentin, N.; Bergwerff, J. A.; Weckhuysen, B. M. *J. Am. Chem. Soc.* **2005**, *127*, 11916−11917.